AIP Advances

RESEARCH ARTICLE | AUGUST 19 2016

# High field-effect mobility at the (Sr,Ba)$SnO_3$/$BaSnO_3$ interface

Kohei Fujiwara; Kazuki Nishihara; Junichi Shiogai; Atsushi Tsukazaki

*AIP Advances* 6, 085014 (2016)
https://doi.org/10.1063/1.4961637

16 April 2024 01:22:28

APL Machine Learning
2023 Papers with Best Practices in Data Sharing and Comprehensive Background
Read Now

AIP ADVANCES **6**, 085014 (2016)

# High field-effect mobility at the $(Sr,Ba)SnO_3/BaSnO_3$ interface

Kohei Fujiwara,[a] Kazuki Nishihara, Junichi Shiogai, and Atsushi Tsukazaki
*Institute for Materials Research, Tohoku University, Sendai 980-8577, Japan*

(Received 7 June 2016; accepted 11 August 2016; published online 19 August 2016)

A perovskite oxide, $BaSnO_3$, has been classified as one of transparent conducting materials with high electron mobility, and its application for field-effect transistors has been the focus of recent research. Here we report transistor operation in $BaSnO_3$-based heterostructures with atomically smooth surfaces, fabricated on $SrTiO_3$ substrates by the $(Sr,Ba)SnO_3$ buffer technique. Indeed, modulation of band profiles at the channel interfaces with the insertion of wide bandgap $(Sr,Ba)SnO_3$ as a barrier layer results in a significant improvement of field-effect mobility, implying effective carrier doping at the regulated heterointerface. These results provide an important step towards realization of high-performance $BaSnO_3$-based field-effect transistors. © *2016 Author(s). All article content, except where otherwise noted, is licensed under a Creative Commons Attribution (CC BY) license (http://creativecommons.org/licenses/by/4.0/).* [http://dx.doi.org/10.1063/1.4961637]

Confining electrons at interfaces offers rich opportunities for exploring quantum transport phenomena as well as for producing novel device concepts based on low dimensionality and high mobility. Recent technological advances in oxide thin-film growth and atomic-scale characterization have brought various oxides into such studies that have been carried out mainly with conventional semiconductors.[1] Among a wide variety of oxides, perovskite-type oxides are one of ideal platforms for such research because various fascinating physical properties including ferroelectricity and ferromagnetism can be incorporated in the common crystal framework. In this context, the recent observation of high electron mobility exceeding 300 $cm^2V^{-1}s^{-1}$ at room temperature in La-doped $BaSnO_3$ single crystals[2] has provided a new arena for building oxide-based heterostructures. Distinct from transition-metal-based perovskites where strong electron correlation and spin-orbit coupling originating from $d$ orbital character play important roles, $BaSnO_3$ possesses a highly dispersive conduction band predominantly composed of Sn 5$s$ orbitals, which leads to relatively small electron effective mass of $0.20m_0$ (where $m_0$ is the free electron mass) and high electron mobility.[3]

One of obvious research targets of the exceptionally high mobility is field-effect transistor (FET) that employs a non-doped $BaSnO_3$ film as the channel. FET allows for electric-field control of high-mobility charge carrier transport at two-dimensional interface as well as practically useful switching function. Because of the lack of appropriate substrates for lattice-matched epitaxy, however, the growth of $BaSnO_3$ films with bulk-like properties remains challenging.[2,4–11] In $BaSnO_3$/$SrTiO_3$(001) with a lattice mismatch of 5.5%, an inevitably formed high density of misfit dislocations was observed by transmission electron microscopy, which is dominant scattering origin for the lower electron mobility in La-doped $BaSnO_3$ films directly grown on $SrTiO_3$(001) than that in single crystals.[5] In those samples, it is also hard to obtain a flat surface, which is another critical issue for the realization of high-performance FET with high-quality gate dielectric/channel interfaces.[5,11] Since the La-doped $BaSnO_3$ channel prepared on $BaSnO_3/SrTiO_3$(001) was confirmed to show FET operation,[12–14] the use of an insulating $BaSnO_3$ buffer effectively enhances FET characteristics owing to reduction of dislocation density in the channel and improvement of surface morphology. In addition, we have recently succeeded in obtaining an atomically smooth

16 April 2024 01:22:28

[a]Author to whom correspondence should be addressed. Electronic mail: kfujiwara@imr.tohoku.ac.jp

 ©Author(s) 2016.

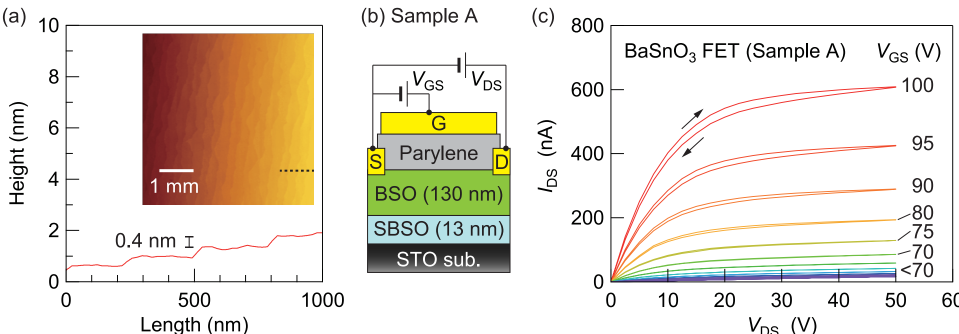


FIG. 1. (a) Typical AFM image and cross-sectional height profile (measured along the dotted line in the image) of atomically smooth $BaSnO_3$ films grown on $Sr_{0.5}Ba_{0.5}SnO_3$ (buffer)/$SrTiO_3$ (001). (b) Schematic device structure of $BaSnO_3$ FET with parylene gate dielectric (Sample A). G, S, D, BSO, SBSO, and STO sub. denote gate, source, drain, $BaSnO_3$, $Sr_{0.5}Ba_{0.5}SnO_3$, and $SrTiO_3$ substrate, respectively. The values in (b) indicate film thicknesses of BSO and SBSO. (c) Output characteristics at room temperature for Sample A.

$BaSnO_3$ surface by introducing $Sr_{0.5}Ba_{0.5}SnO_3$ buffer and high-temperature annealing that mitigate the large lattice mismatch.[11] In this paper, we describe successful FET operation using the non-doped, insulating $BaSnO_3$ channel and enhancement of field-effect mobility $\mu_{FE}$ by engineering the (Sr,Ba)$SnO_3$-based heterointerface.

$BaSnO_3$/$Sr_{0.5}Ba_{0.5}SnO_3$(buffer) multilayers were grown on single-crystalline $SrTiO_3$(001) substrates by pulsed-laser deposition. The film growth was performed using a KrF excimer laser at 900 °C with an oxygen pressure of 0.1 Torr, followed by an *ex-situ* post-annealing at 1200 °C in air.[11] Atomic force microscopy (AFM) observation of the film surfaces, displayed in Fig. 1(a), revealed one-unit-cell height (∼4.1 Å) steps over a wide area. We fabricated a top-gate FET structure on $BaSnO_3$/$Sr_{0.5}Ba_{0.5}SnO_3$(buffer)/$SrTiO_3$(001), schematically shown in Fig. 1(b). The film was patterned into a strip-shaped channel with a width $W$ of 60 µm and a length $L$ of 240 µm by photolithography and Ar ion milling. A gate dielectric layer, an organic polymer parylene-C (relative dielectric constant: $\varepsilon_r = 3.15$),[15,16] with a thickness of ∼480 nm was deposited onto the channel at room temperature. Source, drain, and gate electrodes consisting of Au/Ti bilayers were prepared by electron-beam evaporation. Transport measurements were carried out at room temperature in air with a source-measure unit (Keithley 2614B).

Output characteristics are displayed in Fig. 1(c) as drain current $I_{DS}$ versus drain voltage $V_{DS}$ measured at various gate voltage $V_{GS}$ for the parylene/$BaSnO_3$ device (hereafter referred to as Sample A). The gate leakage current did not exceed 200 pA while $V_{GS}$ was applied. The application of a positive $V_{GS}$ induces an amplification of $I_{DS}$ from the initially insulating channel, demonstrating typical $n$-type FET behavior. Linear $I_{DS}$–$V_{DS}$ relation at low $V_{DS}$ indicates the formation of Ohmic contact between Ti and $BaSnO_3$ under application of gate electric field. Current on/off ratio in the measured $V_{GS}$ range is $\sim 10^4$, which is as large as the values for parylene/$SrTiO_3$[16] and parylene/$KTaO_3$[17] devices fabricated on the bulk single crystal surfaces. Clear saturation behavior at high $V_{DS}$, as well as relatively small $I_{DS}$–$V_{DS}$ hysteresis, corroborates that parylene/$BaSnO_3$ works well as a conducting channel. From the linear region characteristics (as presented below in Figs. 3(c) and 3(d)), $\mu_{FE}$ was estimated to be 8.2 $cm^2V^{-1}s^{-1}$ using the general relation:

$$\mu_{FE} = \frac{\partial I_{DS}}{\partial V_{GS}} \left( \frac{L}{c_i W V_{DS}} \right) \tag{1}$$

where $C_i = 5.8$ $nFcm^{-2}$ is the calculated capacitance per unit area of the parylene gate dielectric with assuming $\varepsilon_r = 3.15$.[15,16] In contrast to previous FETs using La-doped $BaSnO_3$ conducting channels,[12–14] the present FET on non-doped, insulating ones would have an advantage for applications in that a normally-off device with higher current on/off ratio can be developed.

Previous studies aiming at improving characteristics of La-doped $BaSnO_3$ FETs focused on selection of appropriate gate dielectrics and suitable deposition methods that could reduce trap density at the gate dielectric/channel interface.[12–14] In particular, epitaxial $LaInO_3$ barrier/La-doped

16 April 2024 01:22:28

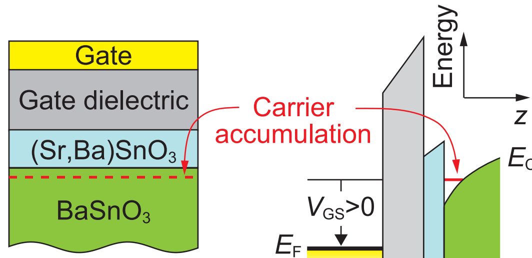


FIG. 2. Schematics of the cross-sectional device structure (left) and conduction band diagram (right) for $(Sr,Ba)SnO_3/BaSnO_3$ heterostructure-based FET proposed in this work. In contrast to the prototype FET, Sample A, in which carriers are induced at the parylene/$BaSnO_3$ interface, conceptually the carriers would be accumulated at the $(Sr,Ba)SnO_3/BaSnO_3$.

$BaSnO_3$ channel revealed high $\mu_{FE}$ of about 90 $cm^2V^{-1}s^{-1}$.[13] Instead of taking such approaches, we attempted to tailor interface band profiles by utilizing bandgap tunability of the $(Sr,Ba)SnO_3$. The *A*-site substitution with isovalent $Sr^{2+}$ in $BaSnO_3$ has been reported to increase the bandgap from 3.50 eV ($BaSnO_3$) to 4.27 eV ($SrSnO_3$) due to the octahedral tilting distortion.[18] In $Sr_{0.5}Ba_{0.5}SnO_3$, bandgap becomes wider by about 0.4 eV than in $BaSnO_3$, while the change in the lattice constant is less than 1%. Although the accurate band alignment of the $(Sr,Ba)SnO_3/BaSnO_3$ system remains to be determined, it is reasonable to assume that large part of the increased bandgap conforms to the conduction band offset since the energy level of the valence band composed mainly of O 2*p* orbitals would be unperturbed so much by cation doping. On the basis of these considerations, we inserted a thin barrier layer of $Sr_{0.5}Ba_{0.5}SnO_3$ to the parylene/$BaSnO_3$ interface. Figure 2 illustrates the cross-sectional schematic of the heterostructure and the plausible band diagram under applying positive $V_{GS}$. The $Sr_{0.5}Ba_{0.5}SnO_3$ barrier likely acts as a dielectric in response to the applied electric field owing to the wide bandgap and conduction band offset. As a consequence, the dominant charge carrier conduction under positive $V_{GS}$ is preferred in the underlying epitaxial $Sr_{0.5}Ba_{0.5}SnO_3/BaSnO_3$ interface. In contrast to the parylene/$BaSnO_3$ interface, the interface scatterings, e.g., by potential fluctuations, are expected to be suppressed by the separation of the conduction channel from the parylene gate dielectric. The concept proposed here essentially resembles the modulation-doping technique used in III-V semiconductor heterostructures.[19]

Figure 3(a) depicts the device structure with a thin $Sr_{0.5}Ba_{0.5}SnO_3$ barrier (Sample B). Using the deposition conditions described above, 7-nm-thick homoepitaxial $BaSnO_3$ and 7-nm-thick $Sr_{0.5}Ba_{0.5}SnO_3$ were regrown on the atomically smooth $BaSnO_3/(Sr,Ba)SnO_3$. Laue fringes up to several orders observed in X-ray diffraction measurement ensure the successful regrowth (see

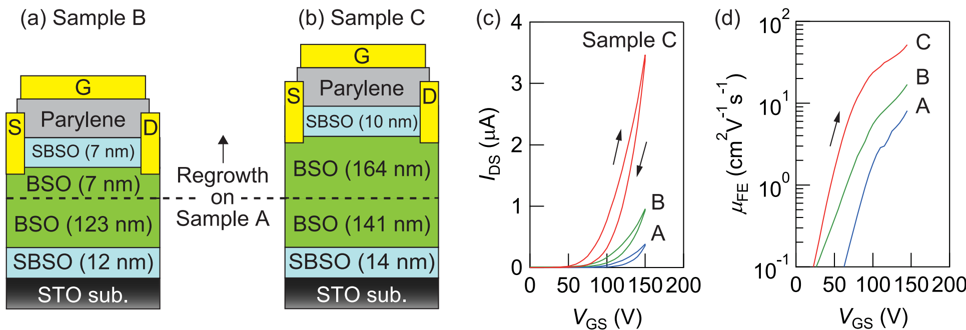


FIG. 3. Schematic device structures of $Sr_{0.5}Ba_{0.5}SnO_3$(barrier)/$BaSnO_3$/$Sr_{0.5}Ba_{0.5}SnO_3$(buffer)/$SrTiO_3$(001) FETs: (a) Sample B with regrown $Sr_{0.5}Ba_{0.5}SnO_3$ barrier (7 nm in thickness) and $BaSnO_3$ (7 nm) layers and (b) Sample C with an increased $BaSnO_3$ thickness (164 nm). To maintain a flat surface for Sample C, an *in-situ* annealing was conducted at 800 °C with an oxygen pressure of $1\times10^{-6}$ Torr for 90 min after depositing half of the regrown layer (82 nm). (c) Transfer characteristics at room temperature measured at $V_{DS} = 1$ V for Samples A (blue), B (green), and C (red). (d) $\mu_{FE}$ calculated from the transfer curves using the relation in the text.

16 April 2024 01:22:28

Fig. S1 in the supplementary material). To detect electrically the embedded interface of top $Sr_{0.5}Ba_{0.5}SnO_3/BaSnO_3$, source and drain electrodes were contacted to $BaSnO_3$ by penetrating the $Sr_{0.5}Ba_{0.5}SnO_3$ barrier with Ar ion milling. In Figs. 3(c) and 3(d), one can see that $I_{DS}$ is in fact increased by the insertion of $Sr_{0.5}Ba_{0.5}SnO_3$ (Samples B and C), which yields $\mu_{FE}$ = 17 $cm^2V^{-1}s^{-1}$ more than twice as high as that for Sample A. As an additional exemplification to exclude the possibility that the carrier accumulation takes place at the parylene/$Sr_{0.5}Ba_{0.5}SnO_3$ interface, we performed a similar measurement on devices in which source and drain electrodes were placed directly onto the $Sr_{0.5}Ba_{0.5}SnO_3$ barrier; however, the electrostatic modulation in conductance was much smaller (Fig. S2 in the supplementary material). In other words, the much larger $I_{DS}$ in Samples B and C than that in Sample A does not originates from the current conduction at the parylene/$Sr_{0.5}Ba_{0.5}SnO_3$ but from the enhancement effect at the $Sr_{0.5}Ba_{0.5}SnO_3/BaSnO_3$. These results strongly support our hypothesis that the conduction channel is preferentially formed in $BaSnO_3$ owing to the band offset effect (Fig. 2).

Another factor that limits charge transport in $BaSnO_3$ films on $SrTiO_3$ is scattering caused by dislocations.[2,5] In our recent study on La-doped $BaSnO_3$ conducting films grown on $BaSnO_3$/$Sr_{0.5}Ba_{0.5}SnO_3$(buffer)/$SrTiO_3$(001),[11] we found that the density of misfit dislocations reaching the top La-doped $BaSnO_3$ layer could be markedly reduced by increasing the thickness of $BaSnO_3$. According to this observation, we prepared Sample C with an increased $BaSnO_3$ thickness shown in Fig. 3(b), resulting in much enhanced mobility of $\mu_{FE}$ = 52 $cm^2V^{-1}s^{-1}$ (Fig. 3(d)). The systematic increase in $\mu_{FE}$ of three device structures is understood to be due to the suppression of extrinsic scatterings at the gate dielectric/channel interface and misfit dislocations.

Figure 4 summarizes the dependence of $\mu_{FE}$ on carrier density $n_{3D}$ for our FETs, together with Hall mobility data reported for La-doped $BaSnO_3$ bulk crystals[4] and films grown on various substrates by pulsed-laser deposition or molecular-beam epitaxy.[4,7,9,11] To perform a fair comparison, the $n_{3D}$ in FETs are estimated from the sheet carrier density given by $C_i$ and $V_{GS}$ and effective channel thickness taking into account the wave function distribution.[20] This analysis is usually applied

16 April 2024 01:22:28

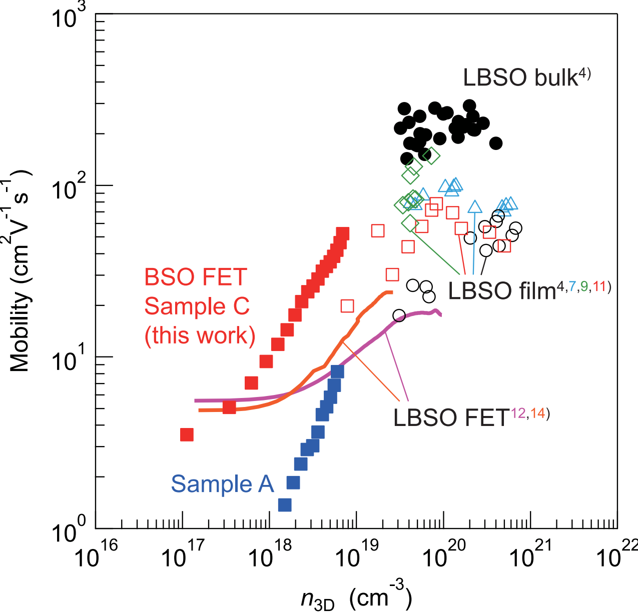


FIG. 4. $\mu_{FE}$ at room temperature as a function of $n_{3D}$ for $BaSnO_3$ FETs (Samples A and C). Hall mobilities at room temperature for La-doped $BaSnO_3$ single crystals (black closed circles), La-doped $BaSnO_3/SrTiO_3(001)$ (Ref. 4) (black open circles), La-doped $BaSnO_3/BaSnO_3(001)$ (Ref. 7) (light blue triangles), and La-doped $BaSnO_3/BaSnO_3/Sr_{0.5}Ba_{0.5}SnO_3$ (buffer)/$SrTiO_3$(001) (Ref. 11) (red open squares) prepared by pulsed-laser deposition, and La-doped $BaSnO_3/PrScO_3(110)$ (Ref. 9) (green diamonds) by molecular-beam epitaxy are plotted for comparison. FETs with La-doped $BaSnO_3$ thin-film channels on $BaSnO_3$ (buffer)/$SrTiO_3$(001) and $Al_2O_3$ (Ref. 12) (purple solid line) and $HfO_2$ gate dielectrics[14] (orange solid line) are also included.

for comparing 2D transport properties with bulk counterparts.[21,22] The values of $\mu_{FE}$ reported for La-doped $BaSnO_3$ FETs are also plotted against $n_{3D}$ calculated by the same procedure using relative permittivity of gate dielectric and sample geometry in literatures.[12,14] On the basis of above assumptions, the estimated $n_{3D}$ corresponds to the upper limit of conducting charge carriers because the number of conducting charge carrier is usually less than the calculated value due to interface trapping and/or low dielectric constant in reality. This plot represents the significance of this work in the following points. At a doping level of $n_{3D} = 6 \times 10^{18}$ cm$^{-3}$, $\mu_{FE}$ of our prototype device, Sample A, is comparable to those of La-doped $BaSnO_3$ FETs; but its much steeper rise in $\mu_{FE}$ against $n_{3D}$ suggests that $\mu_{FE}$ can potentially be higher than them upon further carrier doping. Although the highest value of $\mu_{FE}$ of Sample C with the (Sr,Ba)$SnO_3$-heterostructured channel does not reach the 90 cm$^2$V$^{-1}$s$^{-1}$ of $LaInO_3$/La-doped $BaSnO_3$,[13] it is distinctly high as compared with those values in other La-doped $BaSnO_3$ FETs,[12,14] and, more importantly, seems to be exceeding some Hall mobilities for lightly La-doped $BaSnO_3$ films. To clarify this point, we need Hall effect measurements to evaluate directly the conducting charge carrier density and mobility in future experiment. Considering the absence of ionized impurity scattering in FETs, we envisage that the $\mu_{FE}$ in our FETs may eventually reach and even surpass the high mobility observed in the bulk when further increase of charge carrier density is realized by employing high-$\kappa$ dielectric materials. At least, the dependence of $\mu_{FE}$ on calculated $n_{3D}$ in our FETs manifests large potential of high-mobility channel in $BaSnO_3$ in the low-doping region inaccessible by chemical doping.

In summary, we fabricated FETs with atomically smooth non-doped $BaSnO_3$ channels. We proposed heterointerface engineering with the wide bandgap (Sr,Ba)$SnO_3$ for improving FET characteristics. By suppressing extrinsic scatterings due to ionized impurity, interface roughness, and dislocation, we obtained substantial $\mu_{FE}$ enhancement up to 52 cm$^2$V$^{-1}$s$^{-1}$. The (Sr,Ba)$SnO_3$/$BaSnO_3$ heterointerface as demonstrated here is a promising system for achieving high-mobility electron transport via electrostatic doping. Enhancement in doping capability, e.g., by use of high-$\kappa$ gate dielectric materials such as atomic-layer-deposited $HfO_2$, would lead to further investigation on electronic transport of the high-mobility 5$s$-based electronic state in common perovskite oxide.

16 April 2024 01:22:28

## SUPPLEMENTARY MATERIAL

See Supplementary Material for results of XRD (Fig. S1) and control FET measurements (Fig. S2).

## ACKNOWLEDGMENTS

We would like to thank T. Seki and K. Takanashi for the use of lithography facilities. This work was supported by a Grant-in-Aid for Scientific Research (A) (No. 15H02022) from Japan Society for the Promotion of Science.

[1] H. Y. Hwang, Y. Iwasa, M. Kawasaki, B. Keimer, N. Nagaosa, and Y. Tokura, Nat. Mater. **11**, 103 (2012).
[2] H. J. Kim, U. Kim, H. M. Kim, T. H. Kim, H. S. Mun, B.-G. Jeon, K. T. Hong, W.-H. Lee, C. Ju, K. H. Kim, and K. Char, Appl. Phys. Express **5**, 061102 (2012).
[3] H.-R. Liu, J.-H. Yang, H. J. Xiang, X. G. Gong, and S.-H. Wei, Appl. Phys. Lett. **102**, 112109 (2013).
[4] H. J. Kim, U. Kim, T. H. Kim, J. Kim, H. M. Kim, B.-G. Jeon, W.-J. Lee, H. S. Mun, K. T. Hong, J. Yu, K. Char, and K. H. Kim, Phys. Rev. B **86**, 165205 (2012).
[5] H. Mun, U. Kim, H. M. Kim, C. Park, T. H. Kim, H. J. Kim, K. H. Kim, and K. Char, Appl. Phys. Lett. **102**, 252105 (2013).
[6] P. V. Wadekar, J. Alaria, M. O'Sullivan, N. L. O. Flack, T. D. Manning, L. J. Phillips, K. Durose, O. Lozano, S. Lucas, J. B. Claridge, and M. J. Rosseinsky, Appl. Phys. Lett. **105**, 052104 (2014).
[7] W.-J. Lee, H. J. Kim, E. Sohn, T. H. Kim, J.-Y. Park, W. Park, H. Jeong, T. Lee, J. H. Kim, K.-Y. Choi, and K. H. Kim, Appl. Phys. Lett. **108**, 082105 (2016).
[8] K. Ganguly, P. Ambwani, P. Xu, J. S. Jeong, K. A. Mkhoyan, C. Leighton, and B. Jalan, APL Mater. **3**, 062509 (2015).
[9] S. Raghavan, T. Schumann, H. Kim, J. Y. Zhang, T. A. Cain, and S. Stemmer, APL Mater. **4**, 016106 (2016).
[10] Z. Lebens-Higgins, D. O. Scanlon, H. Paik, S. Sallis, Y. Nie, M. Uchida, N. F. Quackenbush, M. J. Wahila, G. E. Sterbinsky, D. A. Arena, J. C. Woicik, D. G. Schlom, and L. F. J. Piper, Phys. Rev. Lett. **116**, 027602 (2016).
[11] J. Shiogai, K. Nishihara, K. Sato, and A. Tsukazaki, AIP Adv. **6**, 065305 (2016).
[12] C. Park, U. Kim, C. J. Ju, J. S. Park, Y. M. Kim, and K. Char, Appl. Phys. Lett. **105**, 203503 (2014).
[13] U. Kim, C. Park, T. Ha, Y. M. Kim, N. Kim, C. Ju, J. Park, J. Yu, J. H. Kim, and K. Char, APL Mater. **3**, 036101 (2015).

[14] Y. M. Kim, C. Park, U. Kim, C. Ju, and K. Char, Appl. Phys. Express **9**, 011201 (2016).
[15] A. F. Stassen, R. W. I. de Boer, N. N. Iosad, and A. F. Morpurgo, Appl. Phys. Lett. **85**, 3899 (2004).
[16] H. Nakamura, H. Takagi, I. H. Inoue, Y. Takahashi, T. Hasegawa, and Y. Tokura, Appl. Phys. Lett. **89**, 133504 (2006); H. Nakamura, Ph.D. thesis, University of Tokyo, Tokyo, 2007.
[17] H. Nakamura and T. Kimura, J. Appl. Phys. **107**, 074508 (2010).
[18] Q. Liu, B. Li, J. Liu, H. Li, Z. Liu, K. Dai, G. Zhu, P. Zhang, F. Chen, and J. Dai, EPL **98**, 47010 (2012).
[19] T. Mimura, S. Hiyamizu, T. Fujii, and K. Nanbu, Jpn. J. Appl. Phys. **19**, L225 (1980).
[20] T. Ando, A. B. Fowler, and F. Stern, Rev. Mod. Phys. **54**, 437 (1982).
[21] K. Ueno, S. Nakamura, H. Shimotani, A. Ohtomo, N. Kimura, T. Nojima, H. Aoki, Y. Iwasa, and M. Kawasaki, Nat. Mater. **7**, 855 (2008).
[22] C. Bell, S. Harashima, Y. Kozuka, M. Kim, B. G. Kim, Y. Hikita, and H. Y. Hwang, Phys. Rev. Lett. **103**, 226802 (2009).

16 April 2024 01:22:28